HHS Public Access

Author manuscript

NanoImpact. Author manuscript; available in PMC 2020 March 04.

Published in final edited form as:

NanoImpact. 2019 March ; 15: . doi:10.1016/j.impact.2019.100171.

Dispersion preparation, characterization, and dosimetric analysis of cellulose nano-fibrils and nano-crystals: Implications for cellular toxicological studies

Dimitrios Bitounis[a], **Georgios Pyrgiotakis**[a], **Douglas Bousfield**[b], **Philip Demokritou**[a,*]

[a]Center for Nanotechnology and Nanotoxicology, HSPH-NIEHS Nanosafety Center, Department of Environmental Health, Harvard T. H. Chan School of Public School, Harvard University, 665 Huntington Boston, MA 02115, USA

[b]Department of Chemical and Biological Engineering, University of Maine, Orono, ME 04469, USA

Abstract

The characterization of cellulose-based nanomaterial (CNM) suspensions in environmental and biological media is impaired because of their high carbon content and anisotropic shape, thus making it difficult to derive structure activity relationships (SAR) in toxicological studies. Here, a standardized method for the dispersion preparation and characterization of cellulose nanofibrils (CNF) and nanocrystals (CNC) in biological and environmental media was developed. Specifically, electron microscopy was utilized and allowed to specify optimum practices for efficiently suspending CNF and CNC in water and cell culture medium. Furthermore, a technique for measuring the *in vitro* particle kinetics of CNF and CNC suspended in cell culture medium utilizing fluorescently tagged materials was developed to assess the delivery rate of such CNM at the bottom of the well. Interestingly, CNF were shown to settle and create a loosely packed layer at the bottom of cell culture wells within a few hours. On the contrary, CNC settled gradually at a significantly slower rate, highlighting the discordance between administered and delivered mass dose. This work is both novel and urgent in the field of environmental health and safety as it introduces well-defined techniques for the dispersion and characterization of emerging, cellulose-based engineered nanomaterials. It also provides useful insights to the *in vitro* behavior of suspended anisotropic nanomaterials in general, which should enable dosimetry and comparison of toxicological data across laboratories as well as promote the safe and sustainable use of nanotechnology.

Keywords

nanocellulose; nanofibrils; nanocrystals; nanotoxicology; particle kinetics

*Corresponding author: pdemokri@hsph.harvard.edu.

1. Introduction

The natural origin, abundance, and biodegradability of cellulose-based materials have been utilized by the pharmaceutical, food, and construction industries as drug excipients, dietary supplements, and reinforcing abilities in composite materials, respectively (Baiardo et al., 2002; Thoorens et al., 2014; Ullah et al., 2016). Their nanoscale counterparts, termed cellulose-based nanomaterials (CNM), have recently emerged as a potentially sustainable group of materials with enhanced properties. Mechanical strength, high surface to volume area, gas barrier properties, and optical properties impart them with a versatile physicochemical profile that could provide considerably better products in several industrial fields (Cowie et al., 2014; Salas et al., 2014). Intense academic research has been focusing on two main forms of CNM namely cellulose nanofibrils (CNF) and cellulose nanocrystals (CNC) with significant progress being made toward the fabrication of substrates for human stem cell cultures or scaffolds for bone tissue regeneration, modulation of lipid digestion and absorption, and, finally, the production of lightweight and durable films, wound dressings, and food packaging (Cazón et al., 2017; Deloid et al., 2018; Hakkarainen et al., 2016; Lou et al., 2014; Yamaguchi et al., 2016)

CNF can be produced in large quantities using mechanical treatment of cellulosic organic matter, like plant-based biomass, and are semi-crystalline, fibrillar structures (Nechyporchuk et al., 2016). In terms of size, they span several microns in length, but with enough mechanical disintegration and homogenization the diameter of the fibrils may be in the nano-scale (Chinga-Carrasco, 2011). CNC are highly crystalline, rigid nanoparticles of long aspect ratio and their synthesis requires acid hydrolysis of the amorphous part present in CNM (Bondeson et al., 2006; Habibi et al., 2010).

Given the variety of applications and possible economic growth from the use of cellulose-based materials, there has been a lot of interest in profiling their potential pathogenicity (Endes et al., 2016; Ong et al., 2017; Roman, 2015; Zhang et al., 2019). When it comes to microcrystalline cellulose and other types of refined wood pulp, the US Food and Drug Administration (FDA) generally regards them as safe (GRAS) (“Select Committee on GRAS Substances,” 2018). At the same time, the bioactivity and any health risks imposed by CNM exposure are still unknown. This is because the nano-sized features of CNF and CNC may interface with cells and tissues in unpredictable ways, similarly to what has also been hypothesized for other inorganic engineered nanomaterials (ENM) (Chen et al., 2017; Servin and White, 2016; Setyawati et al., 2018; Wu et al., 2013).

The first step toward understanding the interaction of any ENM with living systems is their characterization under conditions which are physiologically relevant to the ENM exposure scenario (Konduru et al., 2018; McClements et al., 2016; Sohal et al., 2018a, 2018b). This task becomes particularly challenging, but all the more important, when ENM are submitted to *in vitro* models of biologically complex processes like ingestion (DeLoid et al., 2017; Guo et al., 2017) and during in vivo studies (Nallanthighal et al., 2017). While it is possible to quantify and characterize cellulose-based materials at high concentrations (several mg/ml) in simple organic and aqueous solvents (Foster et al., 2018; Hubbe et al., 2017; Mao et al., 2017), there is a stark lack of methodological tools for the dispersion preparation and

characterization of CNM suspended at low concentrations (several μg/ml) in complex liquid media, especially culture medium used in *in vitro* cellular studies.

Furthermore, over the last decade, it has become clear that the meaningful interpretation of *in vitro* toxicological studies of ENM requires the reproducible dispersion and characterization of the material to be tested in the dispersant of choice (Cohen et al., 2018, 2014). Indeed, there are numerous works on the importance of good dispersibility of nanoparticles in environmental and biological media, accompanied by a body of literature that attempts to link the physicochemical properties of ENM to their biological activity (Harper et al., 2015; Liu et al., 2013). Although there are tools to understand the deposition and biological effects of aerosolized CNM deposited on cells at the air-liquid interface (Baiardo et al., 2002; Endes et al., 2014), there has been a lack of standardized procedures that describe the dispersion preparation and characterization of low-concentration CNM suspensions for submerged cell cultures.

The limited number of available studies on CNM follow dispersion preparation and characterization methods optimized for metal and metal oxides, but most of these techniques are difficult or inaccurate to adapt to suspensions of particles with such anisotropic shapes, optical, and mechanical properties. Specifically, light-scattering techniques for hydrodynamic size measurements are not optimal for measuring flexible, soft, and fibrous materials (Bloomfield, 2000; Jo et al., 2014; Mao et al., 2017). Furthermore, studies on the colloidal nature of some ENM suspensions have been recently used to quantify the fraction of the administered dose in terms of mass that actually reaches the cells *in vitro* (Cohen et al., 2014; Deloid et al., 2014). This wave of studies culminated with the development of *in silico* models that can be used to estimate delivered to cell dose metrics for any type of near-spherical, rigid nanoparticle (DeLoid et al., 2015; Thomas et al., 2018). In the case of CNM, though, the effect of medium composition on their effective density is not easily quantifiable as inter-particle dynamics cannot be accurately described using numerical models for spherical particles and their sedimentation cannot be based on Stoke's law for rigid bodies undergoing laminar flow.

Here, a first attempt to develop a standardized method for the dispersion preparation and characterization of CNM suspensions in deionized water and cell culture medium is presented. First, we optimized our electron microscopy preparation steps in an effort to obtain an accurate size distribution of the particles suspended in deionized water or cell culture medium. This allowed us to evaluate the effect of sonication and vortexing on dispersing CNM and identify some previously ignored caveats in the preparation of CNM dispersions for cellular studies. Finally, we probed the *in vitro* CNM particle kinetics and dosimetry by employing fluorescence-enhanced CNF and CNC materials recently developed by the authors (Salari et al., 2019). More importantly, the proposed standardized approach across the dispersion preparation, characterization, and dosimetry of CNM in environmental and biological media uncovers traits of CNF and CNC suspensions that should be taken into consideration when performing *in vitro* studies and promotes inter-comparability and standardization in the multi-disciplinary field of nanotoxicology and biomedicine.

2. Materials and method

2.1. Synthesis and characterization of CNF and CNC

The cellulose nano-fibrils (CNF) and cellulose nano-crystals (CNC) used in this study were synthesized according to a procedure described in detail elsewhere by the authors (Pyrgiotakis et al., 2018). In brief, CNF were produced by grinding softwood bleached kraft fibers in an ultra-fine friction grinder. Reverse osmosis water was added to the ground product and the mixture was processed with a disintegrator, resulting in a thick slurry of nano-sized cellulose fibrils. The CNC were synthesized by the hydrolysis of the same kraft fibers in the presence of 72% w/w H_2SO_4. The reaction was quenched with deionized water and neutralized with NaOH. After repeated cycles of washing, the product was a highly-concentrated paste of rigid, spindle-like cellulose crystals. Following their synthesis, both CNF and CNC were autoclaved at 121°C for one hour. The physicochemical characterization of the as-synthesized CNMs was performed by means of electron microscopy (EM), N_2 adsorption, pycnometry, X-ray photoelectron spectroscopy (XPS), Fourier-transform infrared spectroscopy (FTIR), and inductively-coupled plasma mass spectroscopy (ICP-MS).

2.2. Dispersion of CNF and CNC in deionized water and cell culture medium

Both sonication and vortexing were explored as part of developing a standardized protocol for dispersion of CNM. In more detail:

In a 15-ml conical polypropylene tubes, 10 mg of CNF paste (2% w/w dry content) were added in 2.0 ml of deionized water or RPMI-1640 supplemented with 10% fetal bovine serum (FBS) vol/vol, 10 mM HEPES buffer, 100 IU/ml Penicillin, 100 μg ml^{-1} Streptomycin, and non-essential amino acids (1/100 dilution of 100× solution, ThermoFisher) (cell culture medium) to achieve a final concentration of 0.1 mg ml^{-1}. The tubes were sealed with Parafilm, secured on a laboratory vortex mixer using a clamp, and mixed by high-speed vortexing at various timepoints (20s, 60s, 180s, and 600s) in order to parametrically study the effect of vortexing on the dispersibility of CNF. The dispersion of CNF in deionized water was also explored using a calorimetrically calibrated cup-horn sonicator (Branson Ultrasonics, Danbury, CT, USA) as was previously described by Taurozzi et al. (Taurozzi et al., 2011). Specifically, a 2-ml sample of CNF in deionized water at 0.1 mg ml^{-1} was sonicated following the protocol for fast-settling ENM described by Cohen et al. (Cohen et al., 2018) and 389 J were delivered to the suspension.

In order to assess the dispersibility of CNC, 5 mg of CNC paste (4% w/w dry content) were added in 2.0 ml of deionized water or cell culture medium to achieve a final concentration of 0.1 mg ml^{-1}. The tubes were sealed with Parafilm, secured on a laboratory vortex mixer using a clamp, and mixed by high-speed vortexing in order to parametrically assess the effect of vortexing on the dispersibility of CNC.

The effects of vortexing/sonication in the dispersibility of CNF and CNC were then assessed by electron microscopy as described below.

2.3. Electron microscopy of CNF and CNC in deionized water or cell culture medium

Poly-L-lysine (pll) solution (Sigma-Aldrich) was deposited onto 12-mm round mica sheets (Ted Pella Inc.), itself fixed on an aluminum stub. Then, CNF suspended in deionized water or cell culture medium as described above were deposited on the pll-coated mica sheet for 10 minutes. The entire stubs were frozen by placing them on a block of dry ice for at least another 10 minutes and were subsequently submerged in liquid N_2(l) for several seconds to rapidly freeze their entire volume while keeping the fibrils in their native, suspended state. Immediately after freezing in N_2(l), the stub was placed in a flask lyophilizer (Labconco®) where the samples were sublimated overnight at −50 °C and 0.014 mBar. This step removed the frozen liquid while leaving on the stub the frozen fibrils which we could later observe using scanning electron microscopy (SEM) and study their native agglomeration state. Right before imaging, the samples were sputter-coated with a 10-nm layer of Pd/Pt. Electron microscopy was performed using the Everhart-Thornley or in-lens detectors of a Supra 55VPTM field-emission electron microscope (FESEM) by Carl Zeiss AG. The obtained FESEM images of CNF were digitally processed using an ImageJ routine which recorded the projected area A of the two-dimensional particle silhouettes. The equivalent circular area diameter d_a of each particle was then calculated using the formula $d_a = 2(A\ \pi)^{0.5}$ defined as the circle of a diameter d_a that has the same area A as that of the particle (Li et al., 2005). The preparation followed prior to the observation of CNF suspensions in deionized water or cell culture medium by FESEM is summarized in Supplementary Figure 1a.

For the nanoscale characterization of CNC suspended in deionized water, 12 mm round mica sheets (Ted Pella Inc.) fixed on an aluminum stub were sputter-coated with a 10-nm layer of Pd/Pt. This step deposited a flat and thin layer of metals that rendered conductive the surface of the mica sheet. Next, 10 μl of CNC suspended in deionized water as described above were drop cast on the metal-coated mica sheet and left to dry protected from dust. For CNC suspended in cell culture medium, 10 μl of suspension were deposited on the mica sheet. The particles were let to deposit on the meal-coated mica sheet and were left to dry under room temperature to avoid convection currents that could disturb the agglomeration state of the particles. Once dry, 250 μl of deionized water were drop cast on the dried surface. This way, water soluble molecules could re-dissolve in water and distribute across the entire stub while unmasking the CNC on the surface of the mica sheet. Electron microscopy was performed using the in-lens detector of a Supra 55VPTM field emission electron microscope by Carl Zeiss AG. The preparation followed prior to the observation of CNC suspensions in cell culture medium by FESEM is summarized in Supplementary Figure 1b.

2.4. *In vitro* kinetics of CNF and CNC suspended in cell culture medium

Tagging of CNF and CNC with fluorescein isothiocyanate: The covalent bonding of fluorescein isothiocyanate (FITC) on the surface of CNF and CNC and the characterization of the fluorescence-enabled CNMs have been presented in another work from our group (Salari et al., 2019). In brief, CNF and CNC were amine functionalized and then added to a 3.6 mM aqueous FITC solution in the presence of sodium borate and sodium chloride. The materials were then stirred in the dark for several hours to allow FITC to react with the amine groups on the surface of the particles. The covalent bonding of FITC on the

surface of CNF and CNC was verified when there was no more FITC coming off of the particles upon washing.

Cryosectioning of CNM suspensions in cell culture medium to assess kinetics and concentration profiles across the well: In order to estimate the fraction of administered CNF and CNC mass that is progressively deposited on a monolayer of cells ($f_{(D)}$) *in vitro* as a function of time, the particle kinetics of FITC-tagged CNF (FITC-CNF) and FITC-tagged CNC (FITC-CNC) in cell culture medium were assessed following a cryo-sectioning technique developed and used for other nanomaterials by the authors (DeLoid et al., 2015). In summary, cylindrical wells were formed using dental wax (~9.8 mm in height and ~6.3 mm in diameter). These were filled with 1.2 ml of FITC-CNF or FITC-CNC suspended in cell culture medium following the dispersion preparation protocol described above. The choice of dental wax was based on the fact that it is composed of alkanes and other organic molecules which are all insoluble to water. As a result, leaching of material from the dental wax to the contained aqueous-based samples was not considered that it could considerably change their composition. After 0.5, 1.0, and 24.0 hrs, the samples were frozen by placing them on a block of dry ice and then by immersing them in $N_{2(l)}$. The frozen suspensions were removed from their wells by breaking the wax and were sectioned using a Leica CM1850 microtome in 20-μm thick increments. The sections of FITC-tagged CNM suspensions were pooled in groups of 5, thawed, and brought to a final volume of 100 μl with the addition of cell culture medium. Pooling multiple slices allowed us to gain a quantifiable fluorescence signal significantly stronger than the cell culture medium's auto-fluorescence. The samples were transferred to black, clear-bottom, 96-well plates and their fluorescence intensity was recorded by a spectrophotometer equipped with a Xenon lamp (SpectraMax® M5). The recorded signal was then compared against a freshly prepared calibration curve using the same cell culture medium and FITC-tagged CNM. It was thus possible to resolve the concentration of the suspended materials in 100 μm increments at 0.5, 1.0, and 24.0 hours. The space that extends 100 μm from the bottom of the well contains material that has deposited on cells and is of particular importance to in vitro toxicological studies. This space will be hereafter referred to as the "striking zone". Supplementary Figure 2 summarizes the procedure for preparing, sectioning, and measuring the concentration profile of FITC-tagged CNM across the height of wax-based wells. Fluorescence measurements were performed in triplicate for each time-point and fluorescence intensity in each well was measured tree times.

The curves of spatial particle concentration of FITC-CNF and FITC-CNC along the height of the well were fitted at each timepoint using linear and non-linear regression analyses on GraphPad Prism. One-phase decay equations were used for the non-linear regression in the form of $C = (C_0 - P) * e^{-K*l} + P$, where C is the FITC-CNM concentration along the height of the well in μg ml^{-1}, P the plateau of FITC-CNM concentration away from the bottom of the well in μg ml^{-1}, C_0 the initial FITC-CNM concentration of the suspension in μg ml^{-1}, l the distance from the bottom of the well, and K a rate constant. The fraction of administered mass found within the striking zone (f_D) at given exposure times was calculated by integrating the fitted curves over 100 μm along the well's height. The time-resolved evolution of f_D was fitted with a pseudo-first order exponential equation dependent on the

initial concentration of the suspension and tending to a plateau which corresponded to the maximum fraction of mass expected to reach the cells at long timepoints (see results section below). Finally, it needs to be noted that while several in vitro assays are performed over long time-points (e.g., 48 hrs), our preliminary data showed that kinetics of CNF and CNC plateau well before the 12-hour mark. As a result, we did not consider necessary to investigate time-points beyond 24 hours, especially given the laborious nature of the experiment.

3. Results and discussion

3.1. Synthesis and characterization of CNF and CNC

A detailed physicochemical characterization of CNF and CNC can be found in a work previously published by our group (Pyrgiotakis et al., 2018). The quantification of CNF and CNC concentrations in the starting suspensions used to prepare the samples presented in this work has also been independently performed and presented in the work by Pyrgiotakis et al. In summary, the mean diameter of CNF was 50 ± 44 nm. Some of them organized in large, branched structures of which the node-to-node length was 336 ± 233 nm. Free-standing, single fibrils had an average length of 6.710 ± 5.611 μm with an aspect ratio of 107.6 ± 54.5. The specific surface area (SSA) was calculated based on the dimensions of individual fibrils and was found to be 34 m^2 g^{-1}. The average length and diameter of CNC were found to be 267 ± 91 nm and 25 ± 9 nm, respectively. For both CNF and CNC, there were no detectable differences between their chemical composition or surface chemistry and those of wood fibers, as indicated by FTIR, ICP-MS, and XPS analyses. Supplementary Figures 3a and 3b show electron microscopy images of CNF and CNC, respectively. It is worth noting that variations in surface chemistry might affect the dispersibility of CNF and CNC (Yanamala et al., 2016). The CNMs used in this study have been synthesized from a delignified kraft pulp to improve the wettability of the final particles so that the final CNF had a lignin content of ~0.3% w/w. The respective value for CNC would be even lower given that their synthesis through acid hydrolysis is expected to also attack lignin. Furthermore, the surface chemistry of untagged and FITC-tagged CNF and CNC has been shown to be virtually identical under XPS and FTIR (Salari et al., 2019). In fact, the concentration of FITC on CNF and CNC was relatively low at 1×10^{-4} and 4×10^{-5} mol per mol of glucose repeat unit, respectively. As a result, FITC molecules were not expected to significantly affect the sedimentation and diffusion kinetics of CNF and CNC.

3.2. Characterization of CNF and CNC suspended in deionized water and cell culture medium using electron microscopy

A common electron microscopy artefact for soft materials originates from their collapse on electron microscopy substrates. Herein, a sample preparation process that allows fibrils to retain their conformation in deionized water and cell culture medium, thus enabling a more accurate measurement of their size, was developed and utilized as outlined in detail in Materials and Methods. It has to be noted that a biomolecular coating around the observed CNF might increase the apparent size of the agglomerated fibrils. Still, since their size is in the order of tens of microns, this biomolecular coating is not expected to introduce considerable bias. Representative FESSEM images of CNF dispersed in deionized water

with and without our proposed preparation method are included in Supplementary Figure 3c and 3d, respectively. This enhanced preparation allowed us to assess how sonication and vortexing affected their dispersibility in our media of choice as well as how it compared to mixing the material by simple “tube inversion” (see below).

After drop-casting CNC suspended in cell culture medium, the volume of water is removed by evaporation and the amount of crystallizing proteins, amino acids, and small molecules can physically cover CNC on the substrate. The simple preparation process that was introduced prior to FESEM imaging of CNC intersected a step that allowed soluble species to wash away by diffusion, while CNC remained attached on the substrate. Eventually, CNC were uncovered without resorting to wash cycles which could have disturbed the particles’ native agglomeration state. The carbon-based composition of CNC also imparted them with a higher work function than the metal-coated background so that the particles generated high contrast images under FESEM and were easily identifiable.

It is worth noting that when ENM are suspended in liquid media and biological solutions, dynamic light scattering (DLS) is the method of choice for a high-throughput measurement of their hydrodynamic diameter in real time (Murdock et al., 2008). DLS assumes that particles are spherical and scatter light independently of their orientation. Furthermore, the resolution of this technique is limited when measuring the hydrodynamic size of poly-disperse particle populations (Caputo et al., 2019). Specifically, the instrument tends to present data that merge particle populations that are not considerably different in terms of hydrodynamic size. Unfortunately, the flexible and branched structure of CNF on one hand and the long aspect ratio of CNC (~11) on the other, render them unfit for direct measurement by DLS (Khouri et al., 2014; Phan-Xuan et al., 2016). At the same time, traditional preparation steps for the observation of CNM under electron microscopy impose practices that manipulate the composition of the dispersant and the particles’ surface chemistry, as has been previously highlighted (Franken et al., 2017; Ogawa and Putaux, 2018). In our study, we intended to probe the native state of the suspension, therefore using any dispersant other than the environmental and biological media of choice or employing concentrations outside the typical range of nanotoxicology studies was not an option.

3.3. Dispersion optimization of CNF in deionized water and cell culture medium

Effects of sonication during dispersion preparation on cellulose-based nanomaterials: Cup-horn and probe sonication are considered the gold standard for the dispersion of metal and metal oxide ENM in d.i.w and are essential in standardizing methodologies for cellular studies (Bello and Leong, 2017; Cohen et al., 2018). Nevertheless, in this study, sonication of CNF could entangle the fibrils in webs which spanned several μm^2 (Supplementary Figure 4a). Similarly, for CNC here, sonication did not physically alter their shape, but induced some agglomeration, possibly because of increasing the number of inter-particle collisions (Supplementary Figure 4b). Such interdigitated structures of CNM might be useful for some applications, but the smallest possible, discreet nanomaterial structures are required for the reproducibility and standardization of *in vitro*, dose-response studies (Cohen et al., 2013). Consequently, the effect of sonication was deemed unfavorable for dispersing CNF or CNC.

Optimization of vortexing time for CNF: Cellulose nano-fibers should not require a lot of energy to disperse in aqueous-based media due to their surface which is easily wettable by water (Jiang and Hsieh, 2013). Therefore, a low-energy technique like vortexing was explored for dispersing CNF. The optimization of FESEM preparation allowed us to obtain representative images of CNF dispersed in deionized water or cell culture medium. In order to assess their dispersibility, we aimed at measuring several hundreds of these structures from random areas on the stub. Because of the large size of CNF agglomerates, images were captured at relatively low magnification, but to ensure smaller-sized single fibrils were not overlooked, we also captured images at higher magnification.

Figure 1a presents CNF dispersed in deionized water after vortexing of variable duration, while in Figure 1b, higher magnification images suggest there are very few single fibrils present. Figure 1c presents image analysis results in the form of d_A distributions of CNF in deionized water: high-speed vortexing for 20s provided sufficient energy to disperse the CNF in d.i.w at 0.1 mg ml^{-1}. Vortexing for 60 or 180s did not improve the dispersibility of the fibrils, whereas 600s of vortexing appeared to instigate fibril entanglement and shifted the particle size distribution to larger sizes due to the gradual agglomeration of fibrils in shear flow – a phenomenon which has been described in detail elsewhere (Cosgrove, 2009). Even some macroscopically visible structures appeared after 600s of vortexing (shown in Supplementary Figure 4c).

For CNF suspended in cell culture medium at 0.1 mg ml^{-1}, “tube inversion” alone or vortexing for 20s could not thoroughly disperse CNF, as shown in Figures 2a and 2b. On the contrary, 60s of high-speed vortexing resulted in discrete CNF structures, as shown in Figure 2c. Longer vortexing (180s) appeared to re-entangle CNF and generate structures with interweaving borders (Figure 2d). The size distribution of the visualized particles in cell culture medium suggested that CNF agglomerate heavily and form complex structures in the presence of biomolecules. As a result, sub-micron fibrils are not visible and nano-scale features of CNF are masked, possibly due to their coating by proteins and lipids which are abundantly present in FSB-supplemented cell culture media. Here, it should be noted that the overall size of CNF structures in cell culture medium might allow for optical microscopy to be utilized to qualitatively assess the dispersibility of the fibrils, as has been demonstrated by others (Choong et al., 2016).

The systematic testing of the effect of vortexing on CNF dispersed in deionized water suggest that this material can be dispersed using low-energy techniques, but there is an optimum vortexing duration: less vortexing might not deliver enough energy to thoroughly disperse CNF in deionized water or cell culture medium, while over-vortexing is also problematic as it appears to initiate fibril re-entanglement. Finally, it is interesting to notice that fibrils agglomerate in cell culture medium giving rise to structures ~10x larger than those present in deionized water. In toto, the standardized dispersion preparation of CNF in deionized water and cell culture medium is presented in Figure 4a.

3.5. Dispersion optimization of CNC in deionized water and cell culture medium

The rigid structure of CNC excluded the possibility of entanglement and it was thus easier to disperse them than CNF. Furthermore, the CNC surface is covered by sulfonate groups

which readily dissociate in aqueous-based environments and contribute to their hydrophilicity (Chang et al., 2016). Figures 3a and 3b present representative FESEM images of CNC dispersed in water at 0.1 mg ml^{-1} and vortexed for 10s. It was observed that even "tube inversion" alone could adequately disperse CNC in deionized water, but it is suggested to still vortex the suspension in order to standardize the procedure and avoid inter-user variability. The obtained FESEM images present a coffee ring effect typical for sub-micron colloids (Parker et al., 2018): as the drop on the substrate evaporates faster from its shallower edges, liquid flow from the center of the drop toward its periphery carries individual CNC (inset of Figure 3a). When the drop evaporates, most of CNC can be seen piled along the perimeter of the drop, suggesting singly dispersed particles.

Their dispersion in cell culture medium only required 10s of high-speed vortexing to evenly disperse the particles under macroscopic observation. As shown in Figures 3c and 3d, CNC suspended in cell culture medium at 0.1 mg ml^{-1} did not form large agglomerates. However, limited clustering of CNC was present (Figure 3e) which may be attributed to the self-assembly of neighboring CNC at high local concentrations, as has been previously observed for this material (Jiang et al., 2018). In toto, the standardized dispersion preparation of CNC in deionized water and cell culture medium is presented in Figure 4b.

3.6. *In vitro* kinetics of FITC-CNF and FITC-CNF in cell culture medium and effect on dosimetry

As shown in the work by Salari et al., the optimal excitation wavelengths of FITC-CNF and FITC-CNC were 470 and 480 nm, respectively, and both share an emission maximum at 520 nm. For this study, it was determined that their lowest usable concentration in cell culture medium was 5 μg/ml and the smallest sample volume that returned a trustworthy linear relationship between the amount of FITC-tagged CNM and their fluorescence was 100 μl ($R^2 > 0.98$) (data not shown). For both FITC-CNF and FITC-CNC dispersed in cell culture medium, we verified that the recovered material after cryo-sectioning the wells was consistent across all time-points. To do so, we integrated the fitted concentration profiles along the entire length of the well. After performing each measurement in triplicate, the RSD of the recovered FITC-CNC and FITC-CNF were acceptable at 23% and 10%, respectively. The higher RSD for FITC-CNC is attributed to their lower fluorescence intensity which made measurements more susceptible to variations due to background noise.

Concentration profile of FITC-tagged CNF: Figure 5a shows the concentration profile of FITC-CNF along the height of the well at various timepoints. It can be seen that already at 0.5 hrs, the deposited material had occupied 500 μm of the well's height. In fact, CNF appeared to have piled on a layer of constant concentration which will be referred to as the "cloud zone". The progressive formation of the cloud zone is a signal of inefficient packing, probably due to the highly branched structure of CNF and their high specific volume. The rapid settlement of FITC-CNF is in good agreement with the micron-sized structures that were recorded under electron microscopy. Interestingly, FITC-CNF concentration beyond the cloud zone decreased following a one-phase decay as observed for other nano-sized particles, suggesting that shorter, disentangled fibrils remain in suspension for longer times. After 24 hrs, the local concentration of FITC-CNF had increased, indicating that smaller

fibrils had enough time to deposit and/or that the material had slowly rearranged due its flexible and compressible nature.

Fraction of administered mass of FITC-CNF delivered to cell as a function of time (f_D): Figure 5b presents the time-resolved evolution of f_D for FITC-CNF in cell culture medium. Expectedly, f_D at the striking zone only changed marginally (from 0.15 to 0.20) between 0.5 and 1.0 hrs given the material kept piling on top of itself. Following the deposition of smaller fibrils and some rearrangement, its value reached ~0.30 after 24.0 hrs. Overall, these results indicate that within ~1 hour, the material will have quantitatively (>90% of administered mass) deposited in the cloud zone, but only ~30% of the administered mass will be in the vicinity cells, i.e., in the striking zone. The quantitative settling of CNF is explained by the presence of micron-sized agglomerates and the fact that they settle much faster than they diffuse. In other words, Brownian motion is not expected to influence their sedimentation through the cell culture medium used in this study. Having said that, this hydrodynamic behavior is contingent upon the cell culture medium used in this study and significant changes in its composition might also change the settling of CNF. At this point, the packing of the material brings into focus two issues: the first is that particle surface might be a more appropriate metric for dose-response studies of CNF, albeit difficult to calculate; the second is that cells will first come in direct contact with the largest (and faster settling) fraction of the suspended fibrils. Having said that, CNF that have come out of suspension do appear to pack more efficiently with time, suggesting that more fibrils may reach the cells at longer time-points. Also, depending on the cell line, it is possible that some CNF be cleared by phagocytosis, thus allowing new layers of CNF to approach the cells. Eventually, CNF in the cloud zone might move in the striking zone, but the rate and extent of this phenomenon is most likely cell culture medium- cell-, and well-geometry dependent.

Concentration profile of FITC-tagged CNC: Figure 6a shows the concentration profile of FITC-CNC along the height of the well at various timepoints. It can be seen that the concentration of FITC-CNC decreases along the height of the well following a one-phase decay. Moreover, material concentration in the striking zone increases significantly between each time point ($p<0.0001$, regular two-way ANOVA, with subsequent multiple comparisons). Owing to the small volume, rigid structure, and limited agglomeration of FITC-CNC, there is no indication of material piling. Interestingly, the concentration of particles away from the bottom of the tube plateaus below the starting value of 0.1 mg ml^{-1}, indicating that despite its small size and low density, FITC-CNC do not present good colloidal stability in this cell culture medium.

Fraction of administered mass of FITC-CNC delivered to cell as a function of time (f_D): Figure 6b presents the time-resolved evolution of f_D in the striking zone for FITC-CNC in cell culture medium. This material appears to sediment more gradually than FITC-CNF, as expected by its much smaller size. The value of f_D approaches a plateau (0.26), which suggests that only ~26% of the originally administered mass should reach the cells within the context of a 24-hour *in vitro* assay. In contrast to FITC-CNF, it has to be highlighted that the sedimentation of FITC-CNC is expected to depend significantly on the exact composition of the culture medium. Variations in protein content, small molecules, and

viscosity might alter their agglomeration, sedimentation, and diffusion. Therefore, the results presented here should only be regarded specific to the conditions of this study in terms of materials, culture medium, and well geometry. Overall, the *in vitro* employment of CNC should be accompanied by dosimetric considerations in order to achieve meaningful dose-response correlations.

Assuming that cells only interact with materials in the striking zone, overall results suggest that cells will interact with comparable masses of deposited CNF and CNC. For the specific type of CNC used in this study, dispersed in this specific cell culture medium, and contained within the reported well geometry, the mass delivered to cells is ~30% of the administered mass. The mass of CNF deposited in the direct vicinity of cells is also ~30% of the administered mass; at the same time, CNF quantitatively settles out of suspension, but due to its unique morphology does not immediately reach the cells, but rather piles up and forms the cloud zone. To the best of our knowledge, this is the first time that such a behavior is observed for a material with nano-sized features.

4. Conclusion

Cellulose-based nanomaterials are garnering attention from the material science and biomedical fields while their potential applications are most appealing to the pharmaceutical, food, and coatings industries. With this new-found interest in this family of materials, it is also necessary to understand if their long-term use could pose any ill-effects to the environment or human health. Because there are no real-time, high-throughput techniques for the evaluation of CNM suspensions in biologically relevant media, there is equally no systematic characterization prior to their administration to cells, tissues, or animals. In some published studies, characterization data are obtained by techniques that are ideal for metal and metal oxide ENM, but difficult to apply on materials with anisotropic shapes and mechanical properties (e.g., stiffness, homogeneity). It has been established that intercomparable and reproducible toxicological studies require standardized procedures for dispersing, characterizing, and testing ENM. Here, we have optimized some widely adopted material characterization techniques and used them to understand the behavior of CNM suspensions in deionized water and cell culture medium. Specifically, a standardized dispersion preparation process was developed for CNM suspended in deionized water or cell culture medium.

As shown in this study, sonication is not recommended for dispersing CNM, but rather a low energy technique like vortexing is sufficient to disperse them in deionized water and even cell culture medium. Due to the more complex structure of CNF as compared to CNC, there is an optimal vortexing time beyond which fibrils are prone to re-entanglement. At the same time, CNF suspended in cell culture medium organize in fast-settling structures and reach the cells in a matter of a few hours. Consequently, the kinetics of this material in the context of an *in vitro* assay can be summarized by stating that the administered mass equals the mass deposited on cells.

On the contrary, for CNC, dosimetry should be taken into account as the material is expected to progressively deposit on cells over several hours and reach a maximum deposited to cell

dose which is significantly less than the administered dose. Given the numerous physical (length, diameter, aspect ratio, etc.) and chemical (surface chemistry, crystallinity, etc.) synthesizable variants of CNC, the variable composition of cell culture media, and the geometries of in vitro assays, the particle kinetics observed in this study should be regarded as material-, culture medium-, and well-geometry-dependent. Finally, it should be noted that the actual presence of cells may also have an effect on the particle kinetics of CNC, especially if they are actively internalizing deposited material and thus eliminating CNC from the suspension. At the same time, the methods developed to disperse the CNM, characterize them in cell culture media, and measure their kinetics can be employed to study any type of CNC or CNF.

Moving forward, a definite advancement for the field would be to model their kinetics and dosimetry so as to accommodate variable medium composition, well geometry, and particle aspect ratios. In the metrology front, it would be immensely useful to enable real-time particle characterization techniques based on light scattering for particles that veer off the spherical shape onto which their algorithms rely. In the meantime, this work is of value because it emphasizes on some nuances in the preparation and characterization of dilute CNM in deionized water and cell culture medium and also highlights the importance of dosimetric considerations when preforming dose-response studies in submerged cell cultures.

Supplementary Material

Refer to Web version on PubMed Central for supplementary material.

Acknowledgments

The authors would like to acknowledge Emilia Purington for the measurement of FITC molecules on the surface of CNF and CNC.

Research reported in this publication was supported by National Institute of Environmental Health Sciences under Award Number (NIH grant # U24ES026946). The content is solely the responsibility of the authors and does not necessarily represent the official views of the National Institutes of Health. The engineered nanomaterial used in the research presented in this publication have been synthesized, characterized, and provided by the Engineered Nanomaterials Resource and Coordination Core established at Harvard T. H. Chan School of Public Health (NIH grant # U24ES026946) as part of the Nanotechnology Health Implications Research (NHIR) Consortium.

References

Baiardo M, Frisoni G, Scandola M, Licciardello A, 2002 Surface chemical modification of natural cellulose fibers. J. Appl. Polym. Sci 10.1002/app.2229

Bello D, Leong DT, 2017 A decade of nanotoxicology: Assessing the impact on human health and the environment! NanoImpact. 10.1016/j.impact.2017.04.001

Bloomfield VA, 2000 Static and dynamic light scattering from aggregating particles. Biopolymers. 10.1002/1097-0282(200009)54:3<168::AID-BIP20>3.0.CO;2-9

Bondeson D, Mathew A, Oksman K, 2006 Optimization of the isolation of nanocrystals from microcrystalline cellulose by acid hydrolysis. Cellulose. 10.1007/s10570-006-9061-4

Caputo F, Clogston J, Calzolai L, Rösslein M, Prina-Mello A, 2019 Measuring particle size distribution of nanoparticle enabled medicinal products, the joint view of EUNCL and NCI-NCL. A step by step approach combining orthogonal measurements with increasing complexity. J. Control. Release. 10.1016/j.jconrel.2019.02.030

Cazón P, Velazquez G, Ramírez JA, Vázquez M, 2017 Polysaccharide-based films and coatings for food packaging: A review. Food Hydrocoll. 10.1016/j.foodhyd.2016.09.009

Chang H, Luo J, Bakhtiary Davijani AA, Chien AT, Wang PH, Liu HC, Kumar S, 2016 Individually Dispersed Wood-Based Cellulose Nanocrystals. ACS Appl. Mater. Interfaces. 10.1021/acsami.6b00094

Chen H, Zhao R, Wang B, Cai C, Zheng L, Wang H, Wang M, Ouyang H, Zhou X, Chai Z, Zhao Y, Feng W, 2017 The effects of orally administered Ag, TiO2 and SiO2 nanoparticles on gut microbiota composition and colitis induction in mice. NanoImpact. 10.1016/j.impact.2017.07.005

Chinga-Carrasco G, 2011 Cellulose fibres, nanofibrils and microfibrils: The morphological sequence of MFC components from a plant physiology and fibre technology point of view. Nanoscale Res. Lett. 10.1186/1556-276X-6-417

Choong FX, Bäck M, Steiner SE, Melican K, Nilsson KPR, Edlund U, Richter-Dahlfors A, 2016 Nondestructive, real-time determination and visualization of cellulose, hemicellulose and lignin by luminescent oligothiophenes. Sci. Rep 10.1038/srep35578

Cohen J, Deloid G, Pyrgiotakis G, Demokritou P, 2013 Interactions of engineered nanomaterials in physiological media and implications for in vitro dosimetry. Nanotoxicology 10.3109/17435390.2012.666576

Cohen JM, Beltran-Huarac J, Pyrgiotakis G, Demokritou P, 2018 Effective delivery of sonication energy to fast settling and agglomerating nanomaterial suspensions for cellular studies: Implications for stability, particle kinetics, dosimetry and toxicity. NanoImpact. 10.1016/j.impact.2017.12.002

Cohen JM, Teeguarden JG, Demokritou P, 2014 An integrated approach for the in vitro dosimetry of engineered nanomaterials. Part. Fibre Toxicol. 10.1186/1743-8977-11-20

Cosgrove T, 2009 Colloid Science: Principles, Methods and Applications, Colloid Science: Principles, Methods and Applications. 10.1002/9781444305395

Cowie J, Bilek EMT, Wegner TH, Shatkin JA, 2014 Market projections of cellulose nanomaterial-enabled products – Part 1: Applications JO. Tappi J. 10.1038/ncomms11935

Deloid G, Cohen JM, Darrah T, Derk R, Rojanasakul L, Pyrgiotakis G, Wohlleben W, Demokritou P, 2014 Estimating the effective density of engineered nanomaterials for in vitro dosimetry. Nat. Commun 10.1038/ncomms4514

DeLoid GM, Cohen JM, Pyrgiotakis G, Pirela SV, Pal A, Liu J, Srebric J, Demokritou P, 2015 Advanced computational modeling for in vitro nanomaterial dosimetry. Part. Fibre Toxicol. 10.1186/s12989-015-0109-1

Deloid GM, Sohal IS, Lorente LR, Molina RM, Pyrgiotakis G, Stevanovic A, Zhang R, McClements DJ, Geitner NK, Bousfield DW, Ng KW, Loo SCJ, Bell DC, Brain J, Demokritou P, 2018 Reducing Intestinal Digestion and Absorption of Fat Using a Nature-Derived Biopolymer: Interference of Triglyceride Hydrolysis by Nanocellulose. ACS Nano 12, 6469–6479. 10.1021/acsnano.8b03074 [PubMed: 29874029]

DeLoid GM, Wang Y, Kapronezai K, Lorente LR, Zhang R, Pyrgiotakis G, Konduru NV, Ericsson M, White JC, De La Torre-Roche R, Xiao H, McClements DJ, Demokritou P, 2017 An integrated methodology for assessing the impact of food matrix and gastrointestinal effects on the biokinetics and cellular toxicity of ingested engineered nanomaterials. Part. Fibre Toxicol. 14, 40 10.1186/s12989-017-0221-5 [PubMed: 29029643]

Endes C, Camarero-Espinosa S, Mueller S, Foster EJ, Petri-Fink A, Rothen-Rutishauser B, Weder C, Clift MJD, 2016 A critical review of the current knowledge regarding the biological impact of nanocellulose. J. Nanobiotechnology. 10.1186/s12951-016-0230-9

Endes C, Schmid O, Kinnear C, Mueller S, Camarero-Espinosa S, Vanhecke D, Foster EJ, Petri-Fink A, Rothen-Rutishauser B, Weder C, Clift MJD, 2014 An in vitro testing strategy towards mimicking the inhalation of high aspect ratio nanoparticles. Part. Fibre Toxicol. 10.1186/s12989-014-0040-x

Foster EJ, Moon RJ, Agarwal UP, Bortner MJ, Bras J, Camarero-Espinosa S, Chan KJ, Clift MJD, Cranston ED, Eichhorn SJ, Fox DM, Hamad WY, Heux L, Jean B, Korey M, Nieh W, Ong KJ, Reid MS, Renneckar S, Roberts R, Shatkin JA, Simonsen J, Stinson-Bagby K, Wanasekara N,

Youngblood J, 2018 Current characterization methods for cellulose nanomaterials. Chem. Soc. Rev. 10.1039/c6cs00895j

Franken LE, Boekema EJ, Stuart MCA, 2017 Transmission Electron Microscopy as a Tool for the Characterization of Soft Materials: Application and Interpretation. Adv. Sci 10.1002/advs.201600476

Guo Z, Martucci NJ, Moreno-Olivas F, Tako E, Mahler GJ, 2017 Titanium dioxide nanoparticle ingestion alters nutrient absorption in an in vitro model of the small intestine. NanoImpact. 10.1016/j.impact.2017.01.002

Habibi Y, Lucia LA, Rojas OJ, 2010 Cellulose nanocrystals: Chemistry, self-assembly, and applications. Chem. Rev 10.1021/cr900339w

Hakkarainen T, Koivuniemi R, Kosonen M, Escobedo-Lucea C, Sanz-Garcia A, Vuola J, Valtonen J, Tammela P, Mäkitie A, Luukko K, Yliperttula M, Kavola H, 2016 Nanofibrillar cellulose wound dressing in skin graft donor site treatment. J. Control. Release. 10.1016/j.jconrel.2016.07.053

Harper B, Thomas D, Chikkagoudar S, Baker N, Tang K, Heredia-Langner A, Lins R, Harper S, 2015 Comparative hazard analysis and toxicological modeling of diverse nanomaterials using the embryonic zebrafish (EZ) metric of toxicity. J. Nanoparticle Res. 10.1007/s11051-015-3051-0

Hubbe MA, Tayeb P, Joyce M, Tyagi P, Kehoe M, Dimic-Misic K, Pal L, 2017 Rheology of nanocellulose-rich aqueous suspensions: A review. BioResources. 10.15376/biores.12.4.Hubbe

Jiang F, Hsieh Y. Lo, 2013 Chemically and mechanically isolated nanocellulose and their self-assembled structures. Carbohydr. Polym 10.1016/j.carbpol.2013.02.022

Jiang M, McMillan MF, Davis V, Kitchens CL, 2018 Phase Behavior of Acetylated Cellulose Nanocrystals and Origins of the Cross-Hatch Birefringent Texture. Biomacromolecules. 10.1021/acs.biomac.8b00746

Jo Y, Jung J, Lee JW, Shin D, Park H, Nam KT, Park JH, Park Y, 2014 Angle-resolved light scattering of individual rod-shaped bacteria based on Fourier transform light scattering. Sci. Rep 10.1038/srep05090

Khouri S, Shams M, Tam KC, 2014 Determination and prediction of physical properties of cellulose nanocrystals from dynamic light scattering measurements. J. Nanoparticle Res. 10.1007/s11051-014-2499-7

Konduru NV, Damiani F, Stoilova-Mcphie S, Tresback JS, Pyrgiotakis G, Donaghey TC, Demokritou P, Brain JD, Molina RM, 2018 Nanoparticle Wettability Influences Nanoparticle-Phospholipid Interactions. Langmuir. 10.1021/acs.langmuir.7b03741

Li M, Wilkinson D, Patchigolla K, 2005 Comparison of particle size distributions measured using different techniques. Part. Sci. Technol 10.1080/02726350590955912

Liu R, Zhang HY, Ji ZX, Rallo R, Xia T, Chang CH, Nel A, Cohen Y, 2013 Development of structure-activity relationship for metal oxide nanoparticles. Nanoscale. 10.1039/c3nr01533e

Lou Y-R, Kanninen L, Kuisma T, Niklander J, Noon LA, Burks D, Urtti A, Yliperttula M, 2014 The Use of Nanofibrillar Cellulose Hydrogel As a Flexible Three-Dimensional Model to Culture Human Pluripotent Stem Cells. Stem Cells Dev. 10.1089/scd.2013.0314

Mao Y, Liu K, Zhan C, Geng L, Chu B, Hsiao BS, 2017 Characterization of Nanocellulose Using Small-Angle Neutron, X-ray, and Dynamic Light Scattering Techniques. J. Phys. Chem. B 10.1021/acs.jpcb.6b11425

McClements DJ, DeLoid G, Pyrgiotakis G, Shatkin JA, Xiao H, Demokritou P, 2016 The role of the food matrix and gastrointestinal tract in the assessment of biological properties of ingested engineered nanomaterials (iENMs): State of the science and knowledge gaps. NanoImpact. 10.1016/j.impact.2016.10.002

Murdock RC, Braydich-Stolle L, Schrand AM, Schlager JJ, Hussain SM, 2008 Characterization of nanomaterial dispersion in solution prior to in vitro exposure using dynamic light scattering technique. Toxicol. Sci 10.1093/toxsci/kfm240

Nallanthighal S, Chan C, Bharali DJ, Mousa SA, Vásquez E, Reliene R, 2017 Particle coatings but not silver ions mediate genotoxicity of ingested silver nanoparticles in a mouse model. NanoImpact. 10.1016/j.impact.2017.01.003

Nechyporchuk O, Belgacem MN, Bras J, 2016 Production of cellulose nanofibrils: A review of recent advances. Ind. Crops Prod. 10.1016/j.indcrop.2016.02.016

Ogawa Y, Putaux J-L, 2018 Transmission electron microscopy of cellulose. Part 2: technical and practical aspects. Cellulose 0123456789. 10.1007/s10570-018-2075-x

Ong KJ, Shatkin JA, Nelson K, Ede JD, Retsina T, 2017 Establishing the safety of novel bio-based cellulose nanomaterials for commercialization. NanoImpact. 10.1016/j.impact.2017.03.002

Parker RM, Guidetti G, Williams CA, Zhao T, Narkevicius A, Vignolini S, Frka-Petesic B, 2018 The Self-Assembly of Cellulose Nanocrystals: Hierarchical Design of Visual Appearance. Adv. Mater 10.1002/adma.201704477

Phan-Xuan T, Thuresson A, Skepö M, Labrador A, Bordes R, Matic A, 2016 Aggregation behavior of aqueous cellulose nanocrystals: the effect of inorganic salts. Cellulose. 10.1007/s10570-016-1080-1

Pyrgiotakis G, Luu W, Zhang Z, Vaze N, DeLoid G, Rubio L, Graham WAC, Bell DC, Bousfield D, Demokritou P, 2018 Development of high throughput, high precision synthesis platforms and characterization methodologies for toxicological studies of nanocellulose. Cellulose 25, 2303–2319. 10.1007/s10570-018-1718-2 [PubMed: 31839698]

Roman M, 2015 Toxicity of Cellulose Nanocrystals: A Review. Ind. Biotechnol 10.1089/ind.2014.0024

Salari M, Bitounis D, Bhattacharya K, Pyrgiotakis G, Purington E, Gramlich W, Bousfield DW, Demokritou P, 2019 Development and characterization of fluorescently tagged nanocellulose for nanotoxicological Studies. Environ. Sci. Nano

Salas C, Nypelö T, Rodriguez-Abreu C, Carrillo C, Rojas OJ, 2014 Nanocellulose properties and applications in colloids and interfaces. Curr. Opin. Colloid Interface Sci. 10.1016/j.cocis.2014.10.003

Select Committee on GRAS Substances [WWW Document], 2018 . U.S. Food Drug Adm URL https://www.accessdata.fda.gov/scripts/fdcc/?set=SCOGS (accessed 1.1.19).

Servin AD, White JC, 2016 Nanotechnology in agriculture: Next steps for understanding engineered nanoparticle exposure and risk. NanoImpact. 10.1016/j.impact.2015.12.002

Setyawati MI, Sevencan C, Bay BH, Xie J, Zhang Y, Demokritou P, Leong DT, 2018 Nano-TiO2 Drives Epithelial-Mesenchymal Transition in Intestinal Epithelial Cancer Cells. Small. 10.1002/smll.201800922

Sohal IS, Cho YK, O'Fallon KS, Gaines P, Demokritou P, Bello D, 2018a Dissolution Behavior and Biodurability of Ingested Engineered Nanomaterials in the Gastrointestinal Environment. ACS Nano. 10.1021/acsnano.8b02978

Sohal IS, O'Fallon KS, Gaines P, Demokritou P, Bello D, 2018b Ingested engineered nanomaterials: State of science in nanotoxicity testing and future research needs. Part. Fibre Toxicol. 10.1186/s12989-018-0265-1

Taurozzi JS, Hackley VA, Wiesner MR, 2011 Ultrasonic dispersion of nanoparticles for environmental, health and safety assessment issues and recommendations. Nanotoxicology. 10.3109/17435390.2010.528846

Thomas DG, Smith JN, Thrall BD, Baer DR, Jolley H, Munusamy P, Kodali V, Demokritou P, Cohen J, Teeguarden JG, 2018 ISD3: A particokinetic model for predicting the combined effects of particle sedimentation, diffusion and dissolution on cellular dosimetry for in vitro systems. Part. Fibre Toxicol. 10.1186/s12989-018-0243-7

Thoorens G, Krier F, Leclercq B, Carlin B, Evrard B, 2014 Microcrystalline cellulose, a direct compression binder in a quality by design environment - A review. Int. J. Pharm 10.1016/j.ijpharm.2014.06.055

Ullah H, Santos HA, Khan T, 2016 Applications of bacterial cellulose in food, cosmetics and drug delivery. Cellulose. 10.1007/s10570-016-0986-y

Wu YL, Putcha N, Ng KW, Leong DT, Lim CT, Loo SCJ, Chen X, 2013 Biophysical responses upon the interaction of nanomaterials with cellular interfaces. Acc. Chem. Res 10.1021/ar300046u

Yamaguchi K, Prabakaran M, Ke M, Gang X, Chung IM, Um IC, Gopiraman M, Kim IS, 2016 Highly dispersed nanoscale hydroxyapatite on cellulose nanofibers for bone regeneration. Mater. Lett 10.1016/j.matlet.2016.01.010

Yanamala N, Kisin ER, Menas AL, Farcas MT, Khaliullin TO, Vogel UB, Shurin GV, Schwegler-Berry D, Fournier PM, Star A, Shvedova AA, 2016 In Vitro Toxicity Evaluation of Lignin-(Un)coated

Cellulose Based Nanomaterials on Human A549 and THP-1 Cells. Biomacromolecules. 10.1021/acs.biomac.6b00756

Zhang Z, Zhang R, Xiao H, Bhattacharya K, Bitounis D, Demokritou P, McClements DJ, 2019 Development of a standardized food model for studying the impact of food matrix effects on the gastrointestinal fate and toxicity of ingested nanomaterials. NanoImpact 13, 13–25. 10.1016/J.IMPACT.2018.11.002 [PubMed: 31093583]

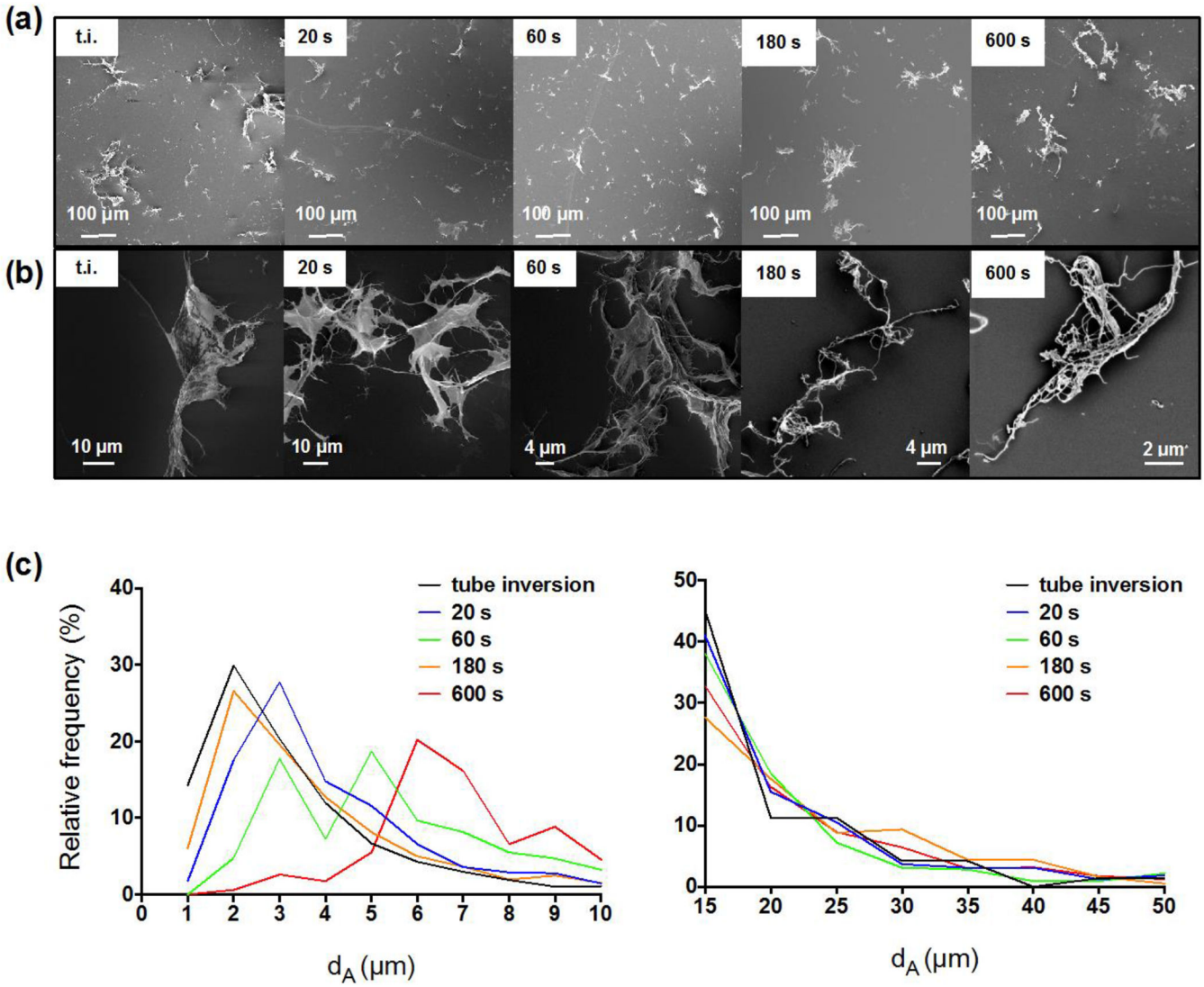

Fig. 1.

Representative FESEM images and d_A frequency distribution of CNF dispersed in deionized water at 0.1 mg ml^{-1}. (a) Representative FESEM images of CNF dispersed in deionized water at 0.1 mg ml^{-1} after "tube inversion" and by applying high-speed vortexing for various durations. (b) Higher magnification images of the samples presented in (a). (c) On the left, the d_A frequency distribution of CNF dispersed in deionized water at 0.1 mg ml^{-1} shows that 20s were enough to disperse the fibrils; more than 180s introduced re-entanglement of small fibrils (1-3 µm) to larger sizes. On the right, the frequency distribution of large agglomerates did not appear to change considerably with various vortexing times. N > 1500 for each timepoint.

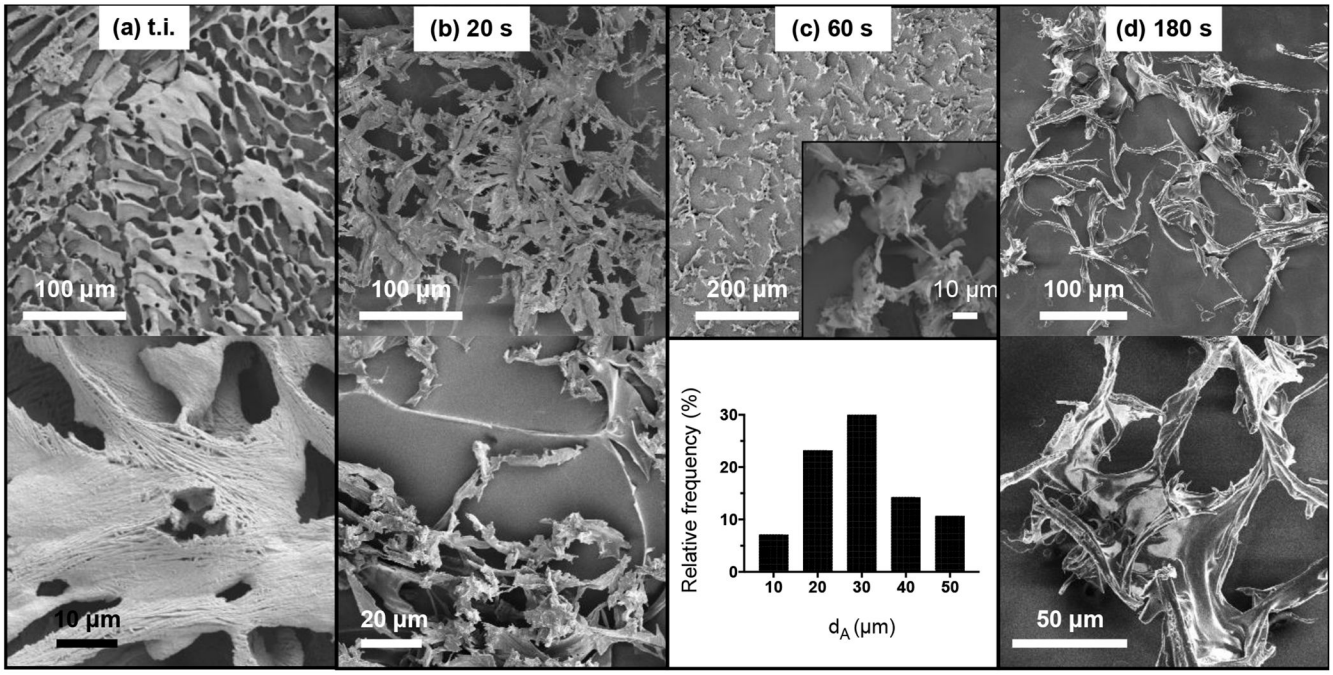

Fig. 2.

Representative FESEM images and d_A frequency distribution of CNF dispersed in cell culture medium at 0.1 mg ml^{-1}. In the top, low magnification FESEM images present heavily interweaved CNF for dispersions prepared by “tube inversion” or vortexing for 20s. Sixty (60) seconds of vortexing were required to generate discreet CNF structures and allow for their size distribution analysis (N =56). Additional vortexing (180s) gave rise to further interweaved macroscale structures.

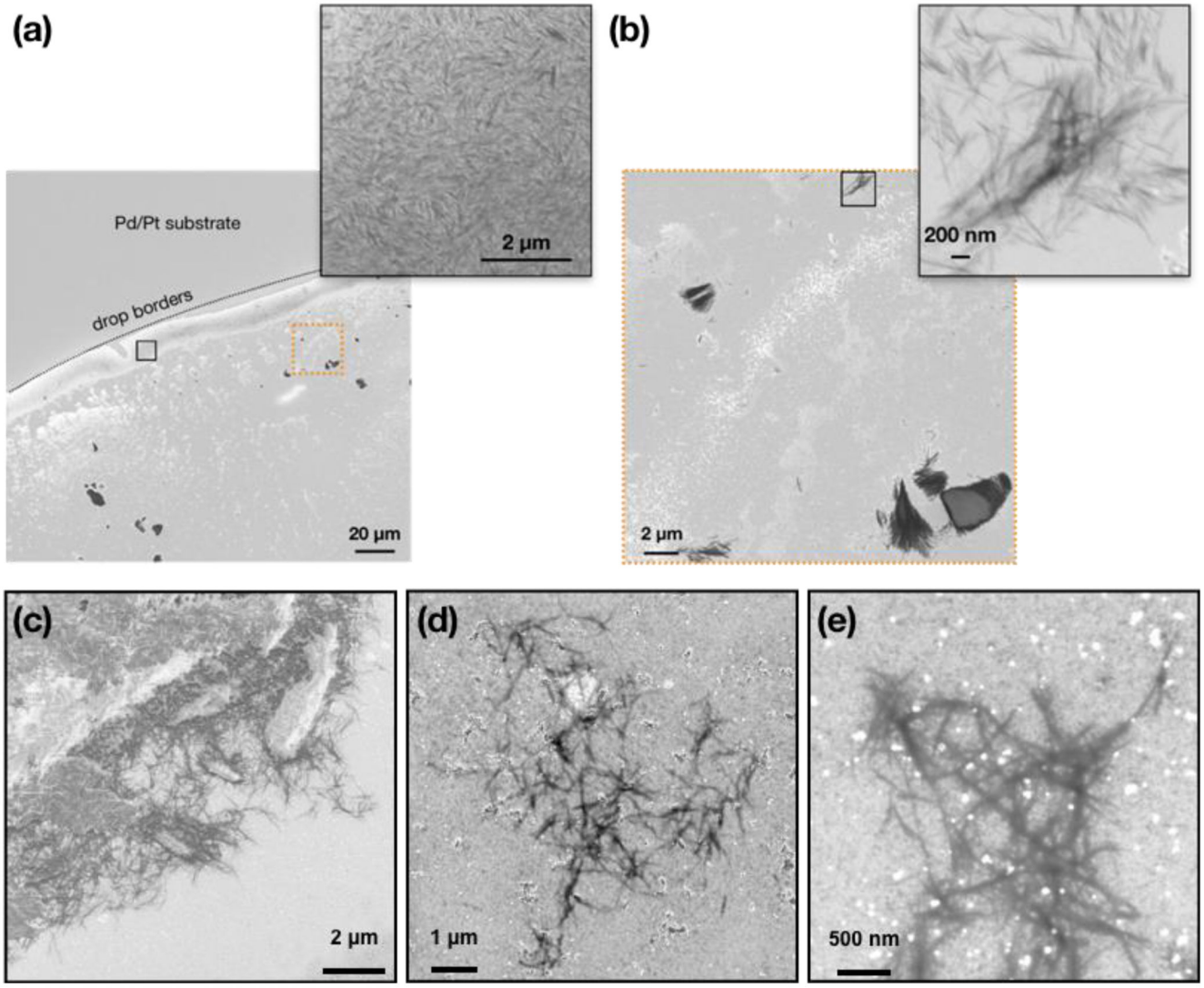

Fig. 3.

Representative FESEM images of CNC dispersed in deionized water and cell culture medium at 0.1 mg ml^{-1}. (a) Low magnification FESEM image presents the outline of the drop that has dried on the Pt/Pd-coated substrate. Accumulation of CNC along the borders of the drop suggests singly dispersed particles (see higher magnification inset of the area in black rectangle). (b) Higher-magnification FESEM images of the area of image (a) enclosed in dashed orange rectangle shows oriented grouping of CNC, as has been reported by others. The inset shows a high-magnification image of the area enclosed in the black rectangle. (c) Low-magnification FESEM images of CNC dispersed in cell culture medium at 0.1 mg ml^{-1} and exposed following the sample preparation procedure presented in the main text. (d-e) Examples of loose CNC clusters observed in cell culture medium.

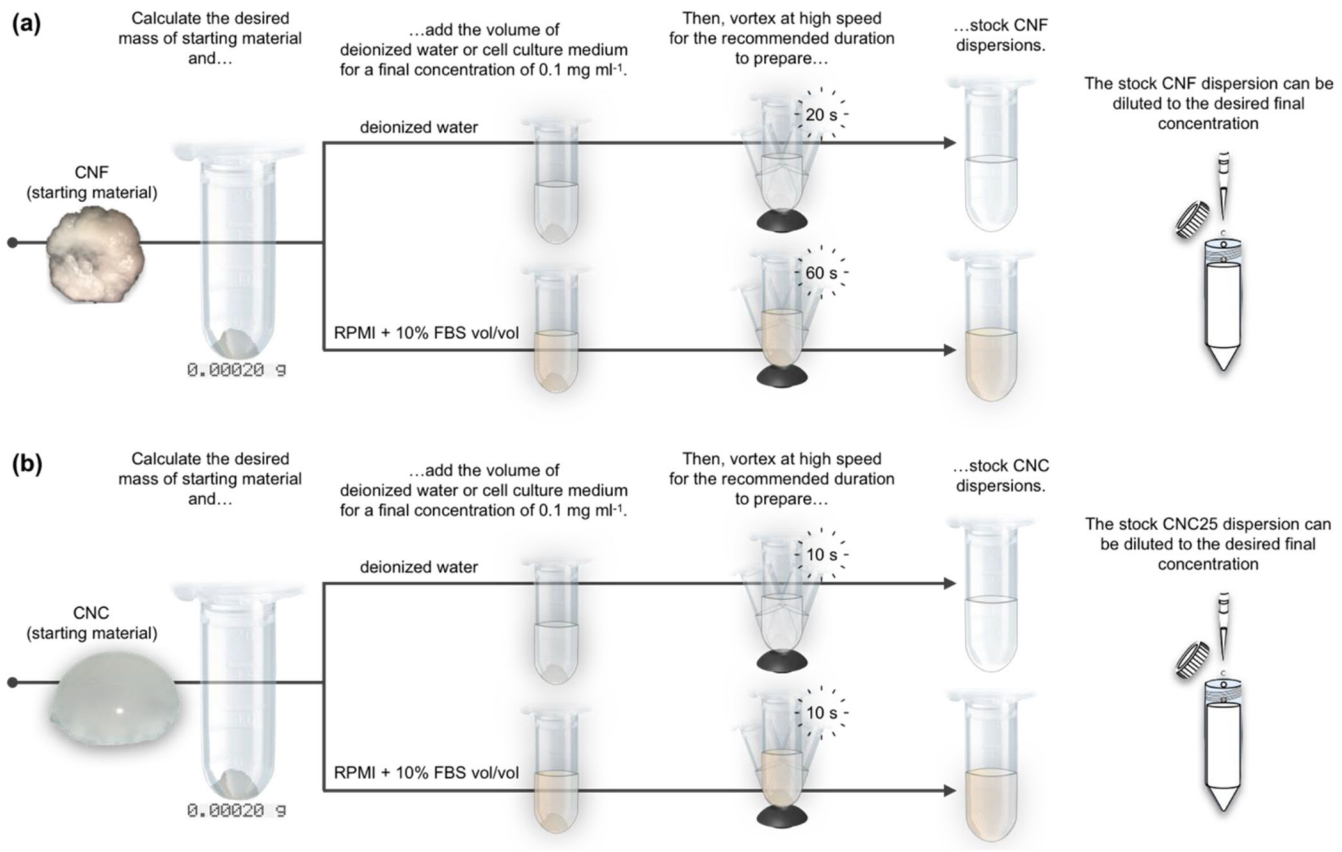

Fig. 4.

Schematics that summarize the dispersion preparation of CNF and CNC in deionized water and cell culture medium. (a) High-speed vortexing for 20 s and 60 s are required for the dispersion preparation of 0.1 mg ml^{-1} CNF in deionized water and cell culture medium, respectively. (b) CNC are easily dispersible and only require 10 s to fully disperse the starting material in deionized water or cell culture medium at a concentration of 0.1 mg ml^{-1}. Freshly prepared dispersions can be readily diluted to lower concentration with the addition of the required amount of dispersant.

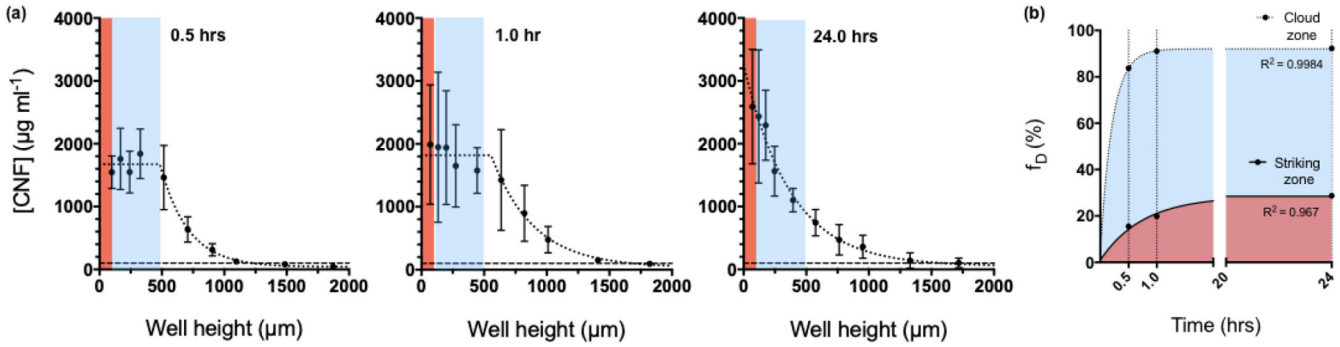

Fig. 5.

Particle kinetics of FITC-CNF in cell culture medium. (a) Time-resolved concentration profile along the height of a well for FITC-CNF dispersed in cell culture medium at 0.1 mg ml^{-1}. The red band indicates the striking zone, i.e., 100 µm of the well's height; the blue band indicates the cloud zone, i.e., the well's height occupied by the total CNF settled out of suspension. At 0.5 and 1.0 hr, the edge of the cloud zone is defined by the change in the spatial concentration profile of FITC-CNF as it shifts from following a linear to a non-linear regression profile. N=3; error bars represent standard deviation from triplicate measurements At 24.0 hrs, the eventual sedimentation of smaller sized fibrils has smoothed the borders of the cloud zone. (b) The fraction of administered dose can be described in terms of the total mass of deposited FITC-CNF (cloud zone – blue band) and the sub-fraction of deposited fibrils in direct vicinity of cells (striking zone – red band). It is interesting to note that the FITC- CNF concentration in the striking zone reaches a plateau later than it does in the cloud zone, suggesting rearrangement and an increase in packing factor of CNF after the material has settled out of suspension.

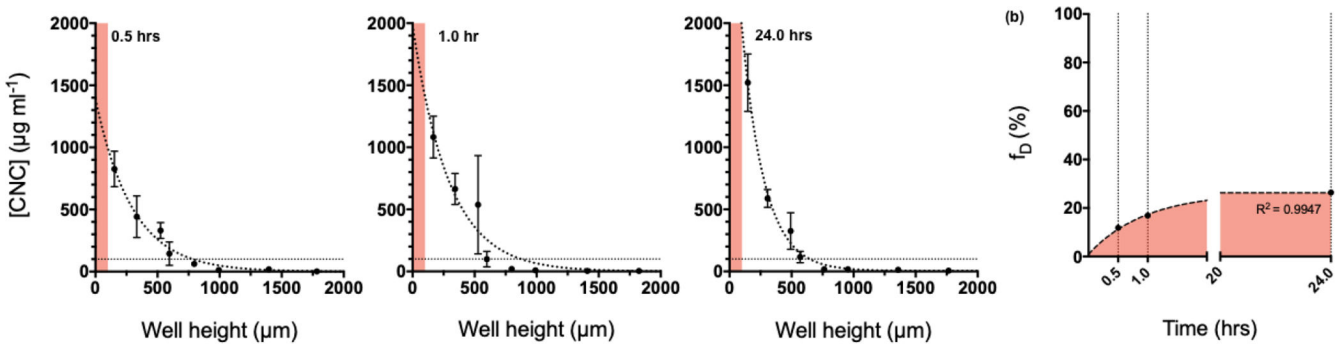

Fig. 6.

Particle kinetics of FITC-CNC in cell culture medium (a) Time-resolved concentration profile along the height of a well for FITC-CNC dispersed in cell culture medium at 0.1 mg ml^{-1}. The red band indicates the striking zone, i.e., 100 μm of the well's height. It is important to note that the FITC-CNC concentration increases significantly between each time point. (b) The fraction of administered mass measured in the striking zone increases gradually, is not expected to surpass more than 0.26 in within a 24-hour in vitro assay.